Physica Medica 68 (2019) 10–16

Contents lists available at ScienceDirect

Physica Medica

journal homepage: www.elsevier.com/locate/ejmp

Original paper

Image quality evaluation of in-treatment four-dimensional cone-beam computed tomography in volumetric-modulated arc therapy for stereotactic body radiation therapy

Yoshinobu Shimohigashi[a,*], Yasuhiro Doi[a], Yumiko Kouno[a], Yohei Yotsuji[a], Masato Maruyama[a], Yudai Kai[a], Ryo Toya[b]

[a] Department of Radiological Technology, Kumamoto University Hospital, Kumamoto, Japan
[b] Department of Radiation Oncology, Kumamoto University Hospital, Kumamoto, Japan

ARTICLE INFO

Keywords:
Gantry rotation speed
Image quality evaluation
In-treatment four-dimensional cone-beam computed tomography
Stereotactic body radiation therapy

ABSTRACT

In this study, the image quality of in-treatment four-dimensional cone-beam computed tomography (In-4D-CBCT) obtained with various prescription doses (PDs) were quantitatively evaluated in volumetric-modulated arc therapy (VMAT) for stereotactic body radiation therapy (SBRT) of the lungs and liver. To assess image quality, we used a dynamic thorax phantom and three-dimensional (3D) abdominal phantom; In-4D-CBCT images were acquired with various PDs (from 5 to 12 Gy). The In-4D-CBCT with various PDs were compared with the reference images (pre-4D-CBCT). The image quality was evaluated using the signal-to-noise ratio (SNR), the contrast-to-noise ratio (CNR), and the Dice similarity coefficient (DSC). The fiducial marker positions with various PDs were compared with those of the reference images. For the dynamic thorax phantom, the difference between pre- and In-4D-CBCT in terms of SNR and CNR decreased, as the PD increased from 6 to 12 Gy. The median DSC ranged from 0.7 to 0.74, and showed good similarity. For the 3D abdominal phantom, the difference between pre- and In-4D-CBCT in terms of SNR and CNR decreased as the PD increased from 5 to 6 Gy; conversely, it increased as the PD increased from 7 to 8 Gy. The fiducial marker positions were within 1.0 mm for all PDs. We concluded that the image quality of In-4D-CBCT degraded compared with the reference image; however, it was sufficiently accurate for assessing the intra-fractional tumor position in VMAT for SBRT of the lungs and liver both in terms of the target volume similarity and accuracy of the fiducial marker position.

1. Introduction

Stereotactic body radiation therapy (SBRT) provides high local control rates with acceptable toxicity for tumors of the lungs and liver [1,2]. Volumetric-modulated arc therapy (VMAT) is a novel rotational technique that allows beam modulation with simultaneous changes in the gantry rotation speed (GRS), dynamic multileaf collimator (MLC) movement, and dose rate; it is applicable for use in SBRT for tumors of the lungs and liver [3,4]. However, to provide accurate SBRT, the inter- and intra-fractional tumor position induced by respiratory motion must be managed during planning simulation and treatment [5–7].

Recently, a system for performing four-dimensional cone-beam computed tomography (4D-CBCT) in a state of delivered treatment megavoltage (MV) beams with gantry rotation, referred to as in-treatment 4D-CBCT (In-4D-CBCT), has been commercialized and used for assessing the intra-fractional position of a moving tumor and for determining the planning target volume (PTV) margin [8,9]. In-4D-CBCT images are reconstructed using the kilovoltage (kV) projection data and respiratory signal acquired during VMAT based on the same principle as 4D-CBCT taken before treatment (pre-4D-CBCT) for target localization [10].

The image quality of 4D-CBCT is known to depend on the number of projection data associated with the GRS [11–13]. Therefore, the image quality of In-4D-CBCT may depend on the prescription doses (PDs) in VMAT plans for SBRT for tumors of the lungs and liver. The GRS in VMAT rotates with non-constant speed according to the treatment plans, and high and low PDs result in slow and fast GRS, respectively. The GRS during acquisition significantly affects the resulting 4D-CBCT image quality [13]. Moreover, projection data acquired during VMAT includes a scatter component arising from treatment MV beams, which may affect the image quality of In-4D-CBCT. Kida et al. investigated the scattering effect of In-4D-CBCT for lung tumor patients and reported

* Corresponding author at: Department of Radiological Technology, Kumamoto University Hospital, 1-1-1 Honjo, Chuo-ku, Kumamoto 860-8556, Japan.
E-mail address: shimohe@kuh.kumamoto-u.ac.jp (Y. Shimohigashi).

https://doi.org/10.1016/j.ejmp.2019.11.003
Received 12 September 2019; Received in revised form 18 October 2019; Accepted 1 November 2019
Available online 11 November 2019
1120-1797/ © 2019 Associazione Italiana di Fisica Medica. Published by Elsevier Ltd. All rights reserved.

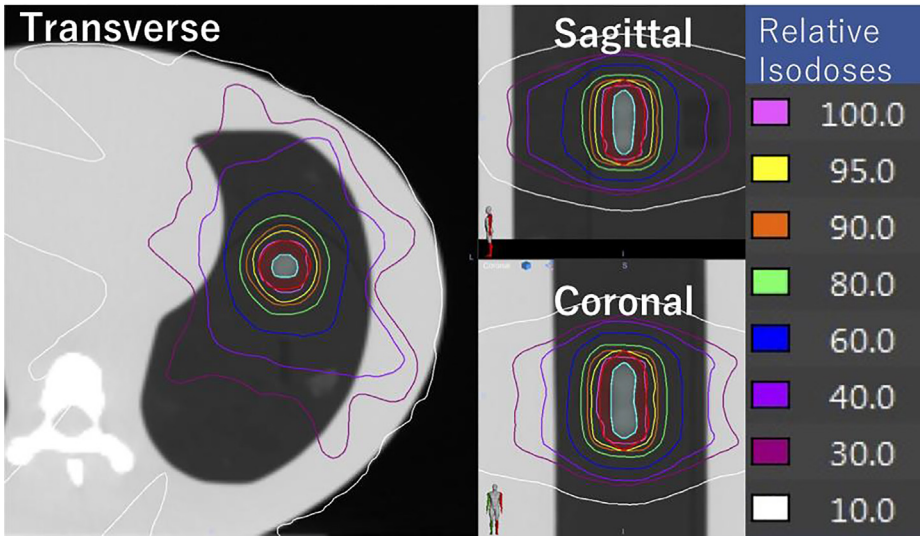

Fig. 1. Dose distribution in a dynamic thorax phantom calculated with a D95 prescription (dose delivered to 95% of planning target volume) of 48 Gy (12 Gy/fraction) using single-arc VMAT for a lung tumor. The internal and planning target volumes are indicated in cyan and red, respectively. (For interpretation of the references to colour in this figure legend, the reader is referred to the web version of this article.)

that there is little effect detectable in the image quality [8]. However, there are no previous reports on the evaluation of image quality of In-4D-CBCT for assessing the intra-fractional tumor position during VMAT in SBRT.

Therefore, the objective of the present study is to quantitatively evaluate the image quality of In-4D-CBCT with various PDs to accurately assess the tumor position in VMAT for SBRT for tumors of the lungs and liver. Here, we investigate the image quality of In-4D-CBCT with various PDs in phantoms of both the lungs and liver.

2. Methods and materials

2.1. Thorax and abdominal phantom

To assess 4D-CBCT image quality, we used a dynamic thorax phantom (Model 008; CIRS Inc., Norfolk, VA, USA) and a three-dimensional (3D) abdominal phantom (Model 057A; CIRS Inc). A spherical target having a diameter of 10 mm inserted in the dynamic thorax phantom sinusoidally moved with respiratory cycles of 4 s and an amplitude of 10 mm along the superior-inferior (SI) direction. A gold fiducial marker (diameter: 2 mm; iGold; Medikit, Tokyo, Japan) was inserted in the vicinity of the liver tumor of the 3D abdominal phantom. The 3D abdominal phantom was then placed over a respiratory motion phantom (QRP Series; Qualita, Nagano, Japan) programmed to move in a sinusoidal waveform with respiratory cycles of 4 s and an amplitude of 10 mm in the SI direction [13,14].

2.2. 4D-CBCT data acquisition

The 4D-CBCT scans were acquired using an X-ray volume imaging (XVI) system (version 5.0.4; Elekta Oncology Systems, Crawley, UK) and the projection data were sorted in 10 respiratory-phase bins [10]. The pre-4D-CBCT images were acquired with exposure parameters of 120 kV, 20 mA, and 16 ms per frame with a GRS of 50°–67° min^{-1} at a field of view (FoV) of 27 cm × 26.4 cm with collimator cassettes of S20. The In-4D-CBCT images were acquired with exposure parameters of 120 kV, 40 mA, and 20 ms per frame with the same FoV used for the pre-4D-CBCT. The image acquisition rate was 5.5 frames/s, and image reconstruction was performed using the Feldkamp filtered back-projection algorithm with a voxel size of 2 mm.

2.3. Phantom assessment

The 4D-CT scans of the thorax and abdominal phantom were acquired using a Discovery RT CT-scanner (GE Healthcare, Chicago, IL), which enables respiratory-synchronized imaging with a real-time position management system (Varian Medical Systems, Palo Alto, CA). The acquisition parameters were set to 120 kV, 70 mA, 0.5-s gantry rotation time, 2.5 mm slice thickness, a FoV of 65 cm, and axial cine mode. The cine durations were set to the respiratory cycles plus the gantry rotation time. The CT images were transferred to the Advantage Sim Workstation (Advantage 4D, GE Healthcare), which sorted the data into 10 phases (0–90%) according to phase-binning algorithms, with 0% and 50% phases corresponding to the maximum inspiration and maximum expiration, respectively. The average intensity projection (AIP) images were generated from the projections obtained for all 10 phases. The internal target volumes (ITVs) were delineated from the target volume of all 10 phases for thorax and abdominal phantoms. The PTV was defined by adding a uniform 5-mm margin to the ITV. All structures of the ITV, PTV, and the organs at risk (OARs; lung, liver, spinal cord, and kidneys) were delineated on the AIP images and exported to a Monaco treatment planning system (version 5.11; Elekta Oncology Systems, Crawley, UK).

Treatment plans for lung tumors were created with a D95 prescription (dose delivered to 95% of PTV) of 48–60 Gy (6, 7.5, 10, and 12 Gy/fraction) using single-arc VMAT with a collimator angle of 15° at a 6 MV photon beam (Fig. 1). Dose constraints for OARs were as follows: the left lung volume received at least 20 Gy < 10% and 5 Gy < 25%; the right lung volume received at least 20 Gy < 0% and 5 Gy < 15%; and the spinal cord volumes received at least 15 Gy < 0% [9]. The number of monitor units (MUs) and segments for the VMAT plans of the lungs with PDs from 6 to 12 Gy ranged from 1345 to 2720 and from 141 to 150, respectively.

Treatment plans for liver tumors were created with a D95 prescription of 35–60 Gy (5, 6, 7, and 8 Gy/fraction) using single-arc VMAT with a collimator angle of 15° at a 6 MV photon beam (Fig. 2). Dose constraints for OARs were as follows: the right and left kidney volumes received at least 25 Gy < 10%; the spinal cord volumes received at least 25 Gy < 0% [15]. The number of MUs and segments for the VMAT plans of the liver with PDs from 5 to 8 Gy ranged from 912 to 1458 and from 120 to 168, respectively. All dose calculations were performed using the X-ray voxel Monte Carlo (XVMC) algorithm with a grid size of 3.0 mm and a standard deviation (SD) of 1% per plan as a convergence criterion [16].

2.4. Image quality evaluation and target position accuracy assessment

Pre-4D-CBCT scans were performed for the phantom setup, and those images were defined as reference images. In-4D-CBCT images with various PDs were compared with reference images using image

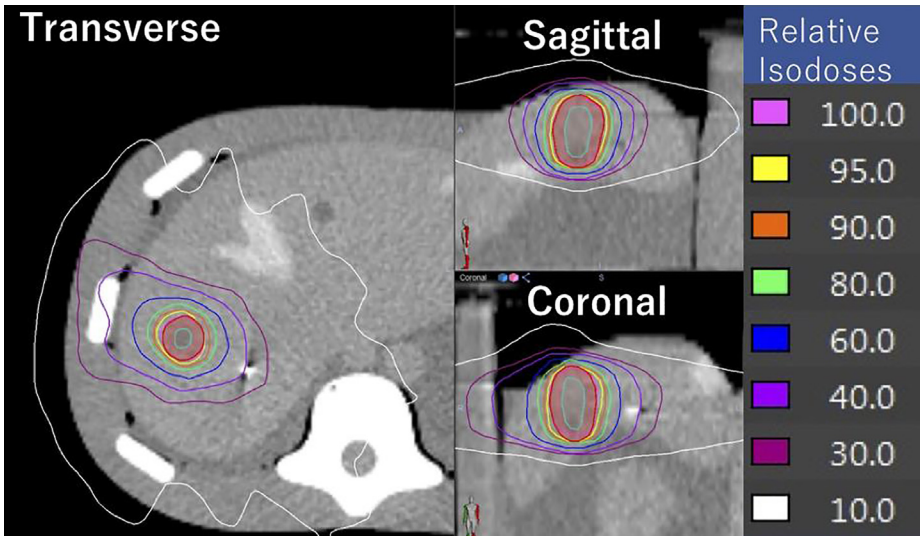

Fig. 2. Dose distribution in a three-dimensional abdominal phantom calculated with a D95 prescription (dose delivered to 95% of planning target volume) of 40 Gy (8 Gy/fraction) using single-arc VMAT for a liver tumor. The internal and planning target volumes are indicated in cyan and red, respectively. (For interpretation of the references to colour in this figure legend, the reader is referred to the web version of this article.)

quality metrics and a target position assessment. The image quality was evaluated by using signal-to-noise ratio (SNR) and contrast-to-noise ratio (CNR) [13,17]. The evaluations were performed in all 10 phases on the 4D-CBCT images.

The SNR was defined over a smooth mediastinum ($R_{mediastinum}$) and liver region (R_{liver}), with a volume of 1 cm × 1 cm (Fig. 3). After measuring the intensities in region (R) using XVI software, the SNR was calculated using the following formula:

$$SNR_i = \frac{Mean(R)_i}{SD(R)_i}, \tag{1}$$

where $Mean(R)_i$ and $SD(R)_i$ denote mean and SD of the intensities in the region at the *i*th phase, respectively.

The CNR was defined based on the intensities of the lung target (T_{lung}) and surrounding lung region (R_{lung}), and the fiducial marker ($T_{fiducial}$) and surrounding liver region (R_{liver}), as shown in Fig. 3, and was calculated using the following formula:

$$CNR_i = \frac{T_i - Mean\ (R)_i}{SD\ (R)_i}, \tag{2}$$

To assess the target position accuracy of In-4D-CBCT images, the Dice similarity coefficient (DSC) and the fiducial marker position were measured using Velocity AI (Varian Medical Systems) and XVI software, respectively. For the target position accuracy of the thorax phantom, the DSC was measured using Velocity AI to evaluate the spatial overlapping of target volumes with pre- and In-4D-CBCT and was calculated using the following formula [18].

$$DSC_i = 2 \times \frac{V_{pre-4Di} \cap V_{In-4Di}}{V_{pre-4Di} + V_{In-4Di}}, \tag{3}$$

where $V_{pre\text{-}4Di}$ and $V_{In\text{-}4Di}$ denote the target volumes in pre- and In-4D-CBCT at the *i*th phase, respectively.

For the abdominal phantom, the fiducial marker position was measured using Elekta XVI software and was based on the center marker position coordinates in all 10 phases of the 4D-CBCT images [13]. The accuracy of the fiducial marker positions was evaluated as the difference between measured positions of pre- and In-4D-CBCT. The root-mean-square errors (RMSEs) of the fiducial marker positions were calculated relative to the reference positions as follows:

$$RMSE = \sqrt{\frac{1}{N}\sum_{i}^{N}(p^i_{In-4D} - p^i_{pre-4D})^2}, \tag{4}$$

where *N* denotes the number of phase bins; and p^i_{In-4D} and p^i_{pre-4D} denote the measured positions of In-4D-CBCT and reference positions of pre-4D-CBCT, respectively, in the *i*th phase bin.

The Kruskal–Wallis test was performed using SPSS Statistics software, version 25.0 (IBM, Armonk, NY, USA) for the statistical analysis of results obtained with various PDs, and a P value < 0.05 was regarded as a significant difference.

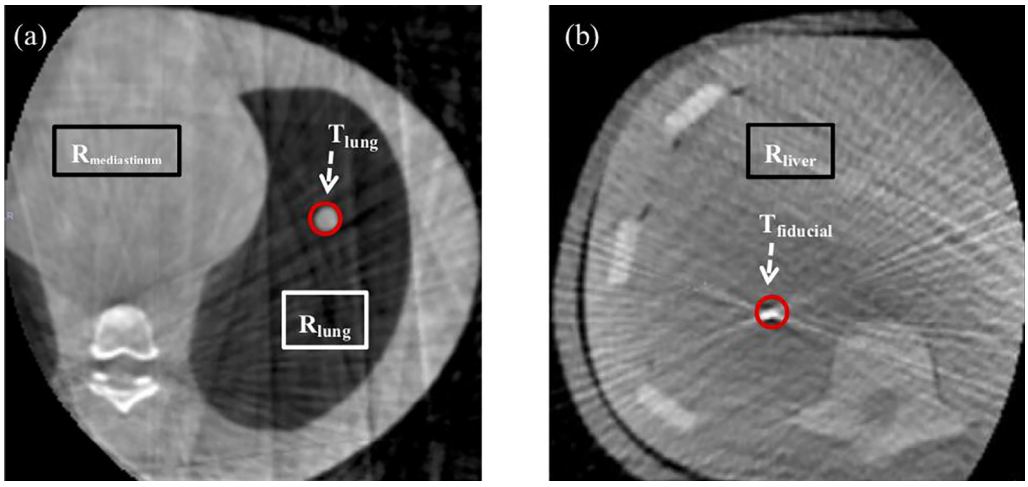

Fig. 3. Image quality assessment of In-4D-CBCT for (a) dynamic thorax phantom and (b) three-dimensional abdominal phantom. The signal-to-noise ratio (SNR) is defined over the smooth mediastinum ($R_{mediastinum}$) and liver region (R_{liver}). The lung target (T_{lung}) and the surrounding lung region (R_{lung}), and the fiducial marker ($T_{fiducial}$) and surrounding R_{liver} are used to calculate the contrast-to-noise ratio (CNR).

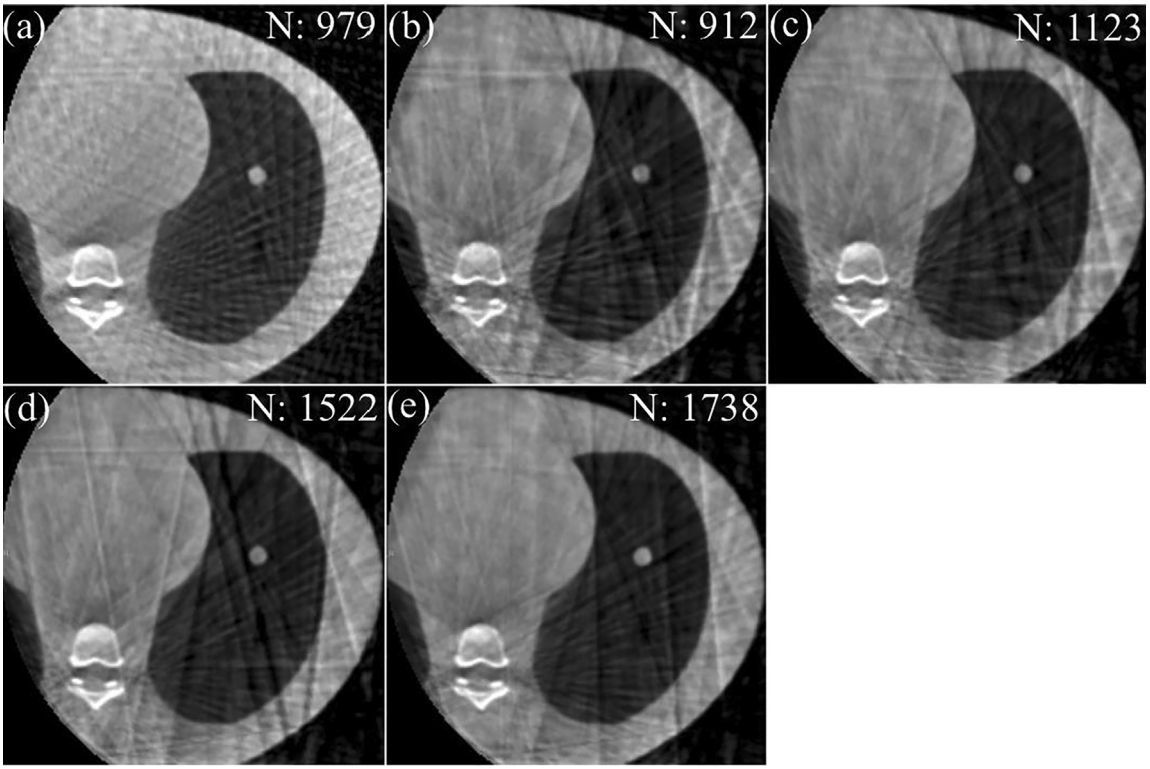

Fig. 4. Pre- (a) and In-treatment 4D-CBCT images (b)–(e) at the phase of maximum expiration for a dynamic thorax phantom. In-treatment 4D-CBCT images are taken at different prescription doses of (b) 6, (c) 7.5, (d) 10, and (e) 12 Gy/fraction. *Abbreviation:* N = total number of projection data.

3. Results

3.1. Phantom assessment

3.1.1. Dynamic thorax phantom

Fig. 4 shows maximum expiration images (50% phase) of pre- and In-4D-CBCT for the dynamic thorax phantom. The streak artifacts on the In-4D-CBCT images decreased as the PD increased from 6 Gy to 12 Gy. The number of projection data for the In-4D-CBCT with PDs from 6 Gy to 12 Gy ranged from 912 to 1738. Meanwhile, the mean and SD of the SNR and CNR increased from 13.3 ± 1.0 to 17.4 ± 1.5 and from 6.5 ± 0.9 to 8.3 ± 1.4, respectively, as the PD increased from 6 Gy to 12 Gy (Fig. 5). The difference between pre- and In-4D-CBCT in terms of SNR and CNR decreased as the PD increased from 6 Gy to 12 Gy. The SNR values differed significantly between the measurements obtained with pre-4D-CBCT versus In-4D-CBCT obtained at 6 Gy ($P = 0.015$). The CNR values differed significantly between the measurements obtained with pre-4D-CBCT versus In-4D-CBCT obtained at 6 Gy ($P < 0.001$)), 7.5 Gy ($P = 0.012$), and 10 Gy ($P = 0.006$). As the PD increased from 6 Gy to 12 Gy (Fig. 5), the median values of the DSC ranged from 0.7 to 0.74, and did not exhibit a statistically significant difference.

3.1.2. 3D abdominal phantom

Fig. 6 shows maximum expiration images (50% phase) of pre- and In-4D-CBCT for the 3D abdominal phantom. Unlike the dynamic thorax phantom, the image quality of the abdominal phantom is compromised by the artifacts generated by the spherical fiducial marker. The amount of projection data for the In-4D-CBCT with PDs from 5 Gy to 8 Gy ranged from 766 to 1019. Meanwhile, the mean and SD of the SNR and CNR increased from 6.5 ± 1.3 to 9.0 ± 1.6 and from 31.3 ± 6.6 to 39.3 ± 6.8, respectively, as the PDs increased from 5 Gy to 6 Gy, but decreased from 8.5 ± 1.3 to 7.5 ± 1.2 and from 36.4 ± 9.2 to 34.0 ± 6.2, respectively, as the PDs increased from 7 Gy to 8 Gy (Fig. 7). The difference between pre- and In-4D-CBCT in terms of SNR and CNR decreased as the PD increased from 5 Gy to 6 Gy; conversely, it increased as the PD increased from 7 Gy to 8 Gy. The SNR values differed significantly between the measurements obtained with pre-4D-CBCT versus In-4D-CBCT obtained at 5 Gy ($P < 0.001$) and 8 Gy ($P = 0.007$). The CNR values did not differ significantly between the measurements obtained with pre-4D-CBCT versus In-4D-CBCT. The mean RMSEs for the fiducial marker positions were 0.63, 0.71, 0.55, and 0.71 mm when the PD was 5, 6, 7, and 8 Gy, respectively.

4. Discussion

We evaluated the image quality of In-4D-CBCT with various PDs to accurately assess intra-fractional tumor position in VMAT for SBRT for tumors of the lungs and liver. For assessment of a dynamic thorax phantom, the image quality increased as the PDs increased. This is because of the increase in the number of projection data because of the slow GRS when the PDs increased. The PD is an important factor affecting the image quality in In-4D-CBCT image acquisition. Takahashi et al. assessed the adequacy of the PTV margin using In-4D-CBCT for fifteen lung cancer patients undergoing VMAT for SBRT with a PD of 50 Gy in 4 fractions (12.5 Gy/fraction) [9]. They found that the intra-fractional tumor position observed by In-4D-CBCT did not exceed 5 mm in any direction for four phases and concluded that In-4D-CBCT is a useful tool for PTV margin determination. In the present study, as shown in Figs. 4 and 5, In-4D-CBCT images obtained with PDs greater than 6 Gy were not visually degraded compared with the reference images (pre-4D-CBCT); the differences in terms of SNR and CNR value decreased. In addition, the DSC used to assess the spatial overlapping of target volumes with pre- and In-4D-CBCT showed good similarity for all PDs. Thus, In-4D-CBCT image obtained with VMAT for lung SBRT was sufficiently accurate for assessing intra-fractional tumor position. However, DSC showed a lower value at an intermediate phase of the respiratory motion where the tumor speed was maximal. Therefore, the

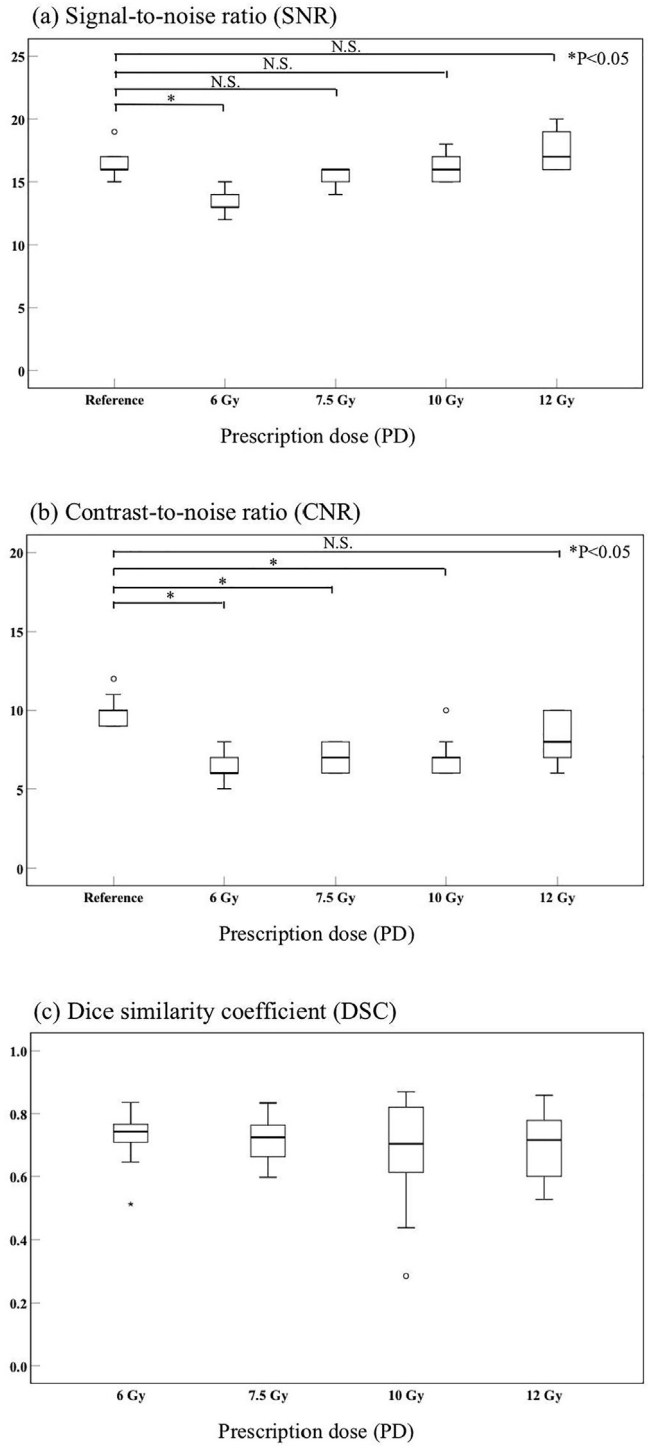

Fig. 5. Box plots of (a) signal-to-noise ratio, (b) contrast-to-noise ratio, and (c) Dice similarity coefficient for In-treatment 4D-CBCT images obtained at different prescription doses for a dynamic thorax phantom. The line in the middle of the boxes represents the median of the image quality metric, and the boxes represent the ranges from the 25th to 75th percentiles. The circles and stars represent the outliers. *Abbreviation:* N.S. = Not significant.

assessment of the tumor position at an intermediate phase may be limited by the respiratory cycles and amplitude of the tumor. Moreover, one of the limitations of the present study is that there was no assessment of the image quality obtained by correcting a scatter component arising from treatment MV beams, as in the study of Kida et al. [8]. However, as shown in Fig. 5, SNR values obtained with PDs greater than 6 Gy used in lung SBRT did not differ significantly compared with the pre-4D-CBCT images without treatment MV beams. Therefore, the scattering effect in In-4D-CBCT for the lung region is believed to be small. This is because the small radiation field used in SBRT and the lack of scattering in the lung region. Kida et al. evaluated image quality for 4 phases of In-4D-CBCT for lung cancer patients and concluded that the image quality of In-4D-CBCT in each phase was not severe enough to preclude identifying the position of tumors [8]. Although we achieved the same result, our study evaluated all 10 phases of In-4D-CBCT images and assessed the intra-fractional tumor position. Moreover, Nakagawa et al. evaluated the image quality of in-treatment 3D-CBCT for the first time and showed that image quality was not visually degraded up to the rotational MV dose of 6 Gy [19]. The present study focuses on In-4D-CBCT images; however, the visual images illustrated in Fig. 4 demonstrate the same trend as their result.

In contrast, for assessment of the 3D abdominal phantom, the image quality in terms of SNR and CNR did not increase as the PDs increased. This is considered to be due to the artifact of the spherical gold fiducial marker, which has high X-ray absorption, and the scattering effect. Thus, the image quality of In-4D-CBCT for liver tumors may change with different fiducial markers; for instance, a coiled fiducial marker is characterized by the visibility on CT scans with fewer image artifacts [20]. Moreover, unlike the lung region, In-4D-CBCT for the liver region may have a greater scattering effect because SNR and CNR values obtained with PD greater than 7 Gy has decreased. Basically, Compton-scattering depends on the electron densities of the tissues (here, lungs and liver) for radiation therapy of the MV photon beams [21]. However, in all PDs, the RMSE of the gold fiducial marker was within 1.0 mm, compared with the pre-4D-CBCT images. Although the image quality of In-4D-CBCT in the liver region degraded compared with the lung region, In-4D-CBCT images obtained with PDs used in VMAT for liver SBRT was sufficiently accurate for the assessment of the intra-fractional tumor position.

The image quality evaluation of In-4D-CBCT in the present study is only a phantom assessment. The VMAT for the phantom study has a simple plan because it has few OARs. However, the clinical patient plan is a complex plan for multiple OARs. In the study of Kida et al. [8], the total number of projection data of In-4D-CBCT for the three lung-tumor patients at 12.5 Gy/fraction are different: the numbers are 649, 945, and 1683. Therefore, the image quality of In-4D-CBCT can be influenced not only by PDs and the scattering effect, but also by the VMAT plan. The image quality of In-4D-CBCT will need to be investigated to ascertain the impact of parameters (mean aperture size, MU, and jaw tracking) and modulation indices (MLC, GRS, and dose rate) on VMAT plans [22]. Moreover, In-4D-CBCT causes additional exposure to patients during VMAT. The doses used with In-4D-CBCT will need to be evaluated in terms of the PDs, the treatment site, and the VMAT plan. Takahashi et al. showed that radiation exposure of In-4D-CBCT was estimated to be as low as 30 mSv per day for lung SBRT with a PD of 50 Gy in 4 fractions [9]. Recently, Gage et al. proposed an approach to generate images of patient anatomy from Compton-scattered photons (Compton scatter imaging) during treatment without additional exposure. Compton scatter imaging exhibits potential for providing the image guidance in lung SBRT [23].

5. Conclusion

In this study, we quantitatively evaluated the image quality of In-4D-CBCT obtained with various PDs for accurately assessing tumor positions in VMAT for SBRT for tumors of the lungs and liver. The PD is an important factor affecting the image quality in In-4D-CBCT image acquisition. Our findings suggest that the image quality of In-4D-CBCT degraded compared with the reference image in terms of SNR and CNR; however, it was sufficiently accurate for assessing the intra-fractional tumor position in VMAT for SBRT of the lungs and liver, both in terms of the target volume similarity and fiducial marker position accuracy.

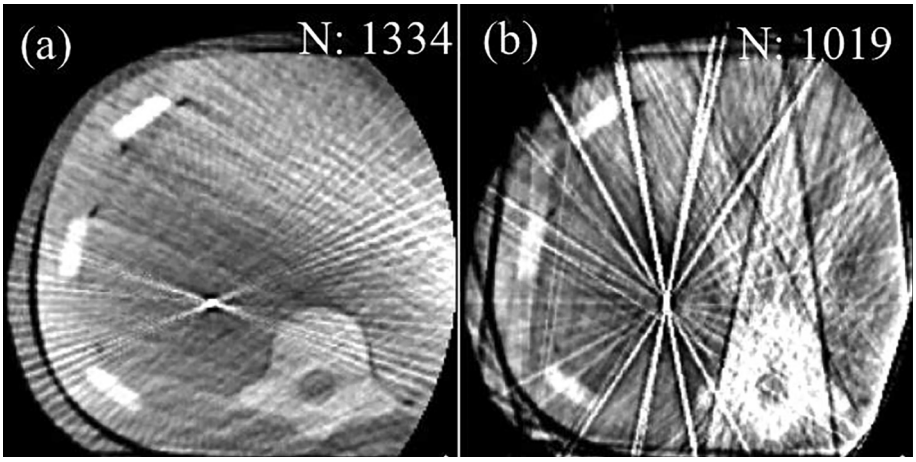

Fig. 6. Pre- (a) and In-treatment 4D-CBCT images (b) at the phase of maximum expiration for a three-dimensional abdominal phantom. In-treatment 4D-CBCT images were taken at a prescription dose of 8 Gy/fraction. *Abbreviation:* N = total number of projection data.

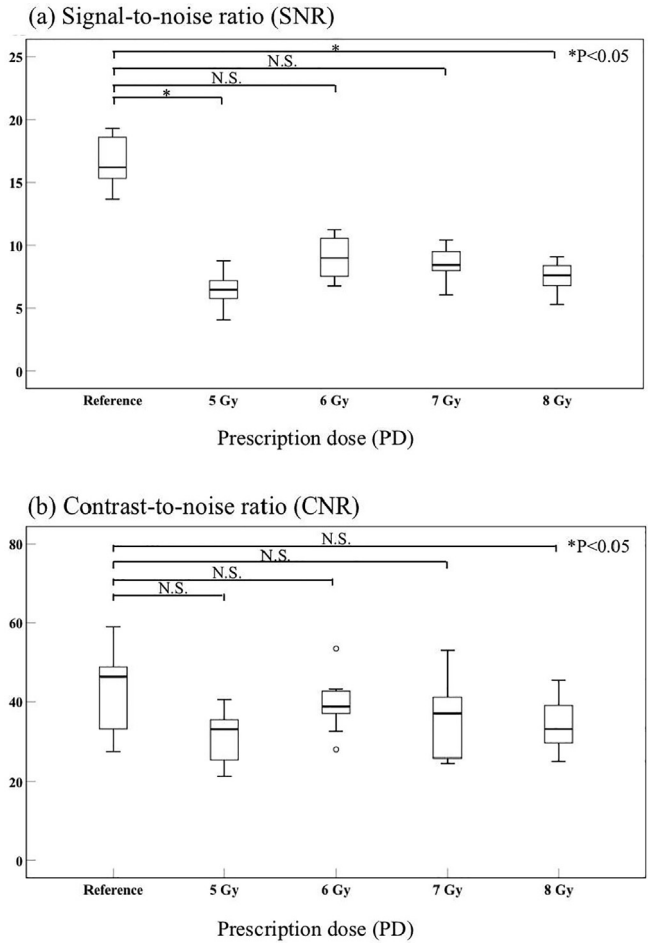

Fig. 7. Box plots of (a) signal-to-noise ratio and (b) contrast-to-noise ratio for In-treatment 4D-CBCT images obtained at different prescription doses for a three-dimensional abdominal phantom. The line in the middle of the boxes represents the median of the image quality metric, and the boxes represent the ranges from the 25th to 75th percentiles. The circles represent the outliers. *Abbreviation:* N.S. = Not significant.

We recommend that In-4D-CBCT be used clinically for high-contrast targets (lung tumors and fiducial markers), taking into account the PD and complexity of the VMAT plans. In-4D-CBCT shows promise as an essential tool for respiratory management of intra-fractional tumor position in SBRT.

Acknowledgment

This work was supported by Japan Society for the Promotion of Science (JSPS) KAKENHI Grant Number JP17K16459.

Conflict of interest

The authors declare that they have no competing interests.

Appendix A. Supplementary data

Supplementary data to this article can be found online at https://doi.org/10.1016/j.ejmp.2019.11.003.

References

[1] Fakiris AJ, McGarry RC, Yiannoutsos CT, et al. Stereotactic body radiation therapy for early-stage non-small-cell lung carcinoma: four year results of a prospective phase II study. Int J Radiat Oncol Biol Phys 2009;75:677–82.
[2] Wulf J, Guckenberger M, Haedinger U, Oppitz U, Mueller G, Baier K, et al. Stereotactic radiotherapy of primary liver cancer and hepatic metastases. Acta Oncol 2006;45:838–47.
[3] Holt A, van Vliet-Vroegindeweij C, Man A, et al. Volumetric-modulated arc therapy for stereotactic body radiotherapy of lung tumors: a comparison with intensity-modulated radiotherapy techniques. Int J Radiat Oncol Biol Phys 2011;81:1560–7.
[4] Jeong Y, et al. Stereotactic body radiation therapy using a respiratory-gated volumetric modulated arc therapy technique for small hepatocellular carcinoma. BMC Cancer 2018;18(1):416.
[5] Michalski D, Sontag M, Li F, de Andrade RS, Uslene I, Brandner ED, et al. Four-dimensional computed tomography-based interfractional reproducibility study of lung tumor intrafractional motion. Int J Radiat Oncol Biol Phys 2008;71:714–24.
[6] Shirato H, Seppenwoolde Y, Kitamura K, Onimura R, Shimizu S. Intrafractional tumor motion: Lung and liver. Semin Radiat Oncol 2004;14:10–8.
[7] Shimohigashi Y, et al. Tumor motion changes in stereotactic body radiotherapy for liver tumors: An evaluation based on four-dimensional cone-beam computed tomography and fiducial markers. Radiat Oncol 2017;12:61.
[8] Kida S, Masutani Y, Yamashita H, et al. In-treatment 4D cone-beam CT with image-based respiratory phase recognition. Radiol Phys Technol 2012;5:138–47.
[9] Takahashi W, Yamashita H, Kida S, et al. Verification of planning target volume settings in volumetric modulated arc therapy for stereotactic body radiation therapy by using in-treatment 4-dimensional cone beam computed tomography. Int J Radiat Oncol Biol Phys 2013;86:427–31.
[10] Sonke JJ, Zijp L, Remeijer P, van Herk M. Respiratory correlated cone beam CT. Med Phys 2005;32:1176–86.
[11] Ahmad M, Pan T. Target-specific optimization of four-dimensional cone beam computed tomography. Med Phys 2012;39(9):5683–96.
[12] Yoganathan SA, Maria Das KJ, Mohamed Ali S, Agarwal A, Mishra SP, Kumar S. Evaluating the four-dimensional cone beam computed tomography with varying gantry rotation speed. Br J Radiol 2016;89:20150870.
[13] Shimohigashi Y, Araki F, Maruyama M, et al. Image quality of four-dimensional cone-beam computed tomography obtained at various gantry rotation speeds for liver stereotactic body radiation therapy with fiducial markers. Phys Med

2018;45:19–24.
[14] Shimohigashi Y, Araki F, Maruyama M, Nakaguchi Y, Nakato K, Nagasue N, et al. Optimization of acquisition parameters and accuracy of target motion trajectory for four-dimensional cone-beam computed tomography with a dynamic thorax phantom. Radiol Phys Technol 2015;8:97–106.
[15] Toya R, et al. Impact of ^{99m}Tc-GSA SPECT image-guided inverse planning on dose-function histogram parameters for stereotactic body radiation therapy planning for patients with hepatocellular carcinoma: A dosimetric comparison study. Dose Response 2019;17(1).
[16] Grofsmid D, Dirkx M, Marijnissen H, Woudstra E, Heijmen B. Dosimetric validation of a commercial Monte Carlo based IMRT planning system. Med Phys 2010;37:540–9.
[17] Shieh CC, Kipritidis J, O'Brien RT, Kuncic Z, Keall PJ. Image quality in thoracic 4D cone-beam CT: A sensitivity analysis of respiratory signal, binning method, reconstruction algorithm, and projection angular spacing. Med Phys 2014;41:041912.
[18] Rodriguez-Romero R, Castro-Tejero P. The influence of respiratory motion on CT image volume definition. Med Phys 2014;41:041701.
[19] Nakagawa K, Yamashita H, Shiraishi K, et al. Verification of in-treatment tumor position using kilovoltage cone-beam computed tomography: a preliminary study. Int J Radiat Oncol Biol Phys 2007;69:970–3.
[20] Hanazawa H, Takahashi S, Shiinoki T, et al. Clinical assessment of coiled fiducial markers as internal surrogates for hepatocellular carcinomas during gated stereotactic body radiotherapy with a real-time tumor-tracking system. Radiother Oncol 2017;123:43–8.
[21] Papanikolaou N, Battista JJ, Pooger AL, et al. Tissue inhomogeneity corrections for megavoltage photon beams. AAPM report no. 85. Madison, WI: Medical Physics Publishing; 2004.
[22] Minsoo C, Hyun JA, Ohyun K, et al. Impact of plan parameters and modulation indices on patient-specific QA results for standard and stereotactic VMAT. Phys Med 2019;62:83–94.
[23] Gage R, Kevin CJ, Alistair T, et al. Compton scatter imaging: a promising modality for image guidance in lung stereotactic body radiation therapy. Med Phys 2018;45(3):1233–40.